Available online at www.sciencedirect.com
ScienceDirect
European Journal of Medicinal Chemistry 44 (2009) 785–793
EUROPEAN JOURNAL OF MEDICINAL CHEMISTRY
http://www.elsevier.com/locate/ejmech

Original article

Some O,O',O'',O'''-di/tetra aryldithioimidophonate transition metal complexes derived from catechol and bisphenol-A as antibacterial and antifungal agents

Vikrant Kumar [a], Tansir Ahamad [b], N. Nishat [a,*]

[a] Department of Chemistry, Faculty of Natural Sciences, Jamia Millia Islamia (Central University), New Delhi 110025, India
[b] Departments of Chemistry and Polymer Science, Stellenbosch University, Stellenbosch 7602, South Africa

Received 24 March 2007; received in revised form 17 April 2008; accepted 17 April 2008
Available online 29 April 2008

Abstract

Two new substituted-thioimidophonate derivatives H_1L_1 (O,O',O'',O'''-diaryldithioimidophonates) and H_1L_2 (O,O',O'',O'''-tetra aryldithioimidophonates) were synthesized. These thioimidophonates are potential ligands towards transition metal ions. The reaction of M(II) acetates (M(II) = Mn(II), Co(II), Ni(II), Cu(II), and Zn(II)) with H_1L_1 and H_1L_2 resulted in the formation of solid complexes with the composition $(L_1/L_2)_2M(II)$. These compounds were characterized through elemental analysis, electrical conductance, infrared, electronic spectra, nmr, magnetic susceptibilities etc. Vibrational mode assignments of ν(PN), ν(PS), ν(MS), phenyl and methyl group bands are made. Structural and bonding changes are correlated with these vibrational frequencies. All the compounds were screened for their antibacterial and antifungal properties and have exhibited potential activities with MIC (0.09–1.50 μg/ml).

Keywords: Phonate metal complexes; Antibacterial and antifungal activities

1. Introduction

Compounds containing N, O, and S donor groups and their metal complexes play a key role in understanding the coordination chemistry of transition metal ions [1–3]. This is due to remarkable biological activities observed for these compounds, which have since been shown to be related to their metal complexing ability. These compounds present a great variety of biological activities ranging from antitumor to fungicide, bactericide, anti-inflammatory, and antiviral activities [4–8]. Compared to the number of metal β-diketonate (and other similar bidentate O-donor anions), relatively few structural examples of bidentate S donor analogues have been reported [9,10]. Bidentate S-donor ligands such as dithioimidophosphinate ($R_2XPNXPR_2$) where R = CH_3 or C_6H_5 and X = S, O, or NH, were first synthesized by Schmidpeter et al [11–13]. Structure and bonding in dithioimidophosphinate (L) ligands make them unique among sulfur donors in several respects: (1) stereo chemical trends in $M''L_2$ complexes, M = first-row transition metal; (2) redox behavior of metal and ligand in complex formation; and (3) nonrigidity of chelate ring geometry. The four-coordinated geometry about P atoms of ligand was expected to produce appropriate puckering of six-membered chelate rings in $M''L_2$ complexes and so, possibly, induce tetrahedral and square planar geometries about the central metal atom [14]. The potentialities of tetra-alkyl substituted dithioimidophonates as powerful complexing agents for zinc from aqueous solution with good selectivity over iron [15] were recently recognized by Morley and Bonford and co-workers. Similarly plenty of articles with aryl substituted dithioimidophonates along with their applications have been reported [16,17]. It is well known that some drugs have increased activity when administered as metal complexes than as free organic compounds [18]. On the other hand a large number of stability problems encountered with

* Corresponding author. Tel.: +91 11 2682 3254; fax: +91 11 2684 0229.
E-mail address: nishat_nchem03@yahoo.co.in (N. Nishat).

0223-5234/$ - see front matter © 2008 Elsevier Masson SAS. All rights reserved.
doi:10.1016/j.ejmech.2008.04.008

organic moiety would be avoided by the use of transition metal complexes. A large number of reports are available on the chemistry and the biocidal activities of transition metal complexes containing O, N and S donor atoms. So far, the coordination of sulfur with transition metals has been explored more thoroughly than its coordination with nontransition metals [19].

The various factors discussed above, particularly biological activities of substituted transition metal complexes prompted us to prepare new derivatives of thiophonates using a simple and efficient method. The present communication reports the synthesis and structural elucidation by various physicochemical methods of a series of compounds which were then subjected to *in vitro* antibacterial and antifungal activities against some pathogens.

2. Syntheses

2.1. Synthesis of chloride derivatives of precursor compounds

*2.1.1. Synthesis of chloride derivative of precursor compound **1** (PC_1-Cl)*

A solution of (44 g, 0.4 mol) catechol and sodium hydroxide solution (16.0 g, 0.4 mol in 24 mL water) was added into 80 mL benzene under vigorous stirring. Benzyl triethyl ammonium chloride (BTAC) (1.2 mmol), a phase transfer catalyst (PTC) was added to the reaction mixture and simultaneously $PSCl_3$ (34 g, 0.2 mol) was added dropwise from the additional funnel over a period of 30 min. Stirring of the reaction mixture was continued and progress of the reaction was monitored by TLC. A separating funnel was used to separate the mixed organic phase followed by the addition of 100 ml water. The organic phase was washed with water until pH = 7, it was dried over anhydrous Na_2SO_4 and evaporated. After evaporation of the solvent, the residue was purified and recrystallized affording stable crystals (Scheme 1).

PC_1-Cl: empirical formula $C_6H_4O_2SPCl$, yield 71.0%, m.p. 64–65 °C. ^{1}H NMR (300 MHz, DMSO, δ) 7.12 (m, 4H, ArH). FT-IR (KBr pellets ν_{max} cm^{-1}) 1600, 1560, 1185, 750. Anal.% (found): C (34.87), H (1.96), S (15.49), Cl (17.15).

*2.1.2. Synthesis of chloride derivative of precursor compound **2** (PC_2-Cl)*

The chloride derivative of PC_2 was synthesized by the reaction of bisphenol-A with $PSCl_3$. Bisphenol-A (15.52 g, 0.4 mol) and NaOH (16.0 g, 0.4 mol in 24 ml water) solution were added to 80 ml benzene under vigorous stirring, then 1.2 mmol BTAC was added into this reaction mixture with dropwise addition of $PSCl_3$ (3.4 g, 0.02 mol). Progress of the reaction was monitored by thin layer chromatography (TLC). This mixture was further treated in the same manner as in Scheme 1.

PC_2-Cl: empirical formula $C_{15}H_{14}O_2PSCl$, yield 75%, m.p. 70–72 °C. ^{1}H NMR (300 MHz, DMSO, δ) 6.96–7.01 (m, 8H, ArH), 1.63 (m, 6H, CH_3). FT-IR (KBr pellets ν_{max} cm^{-1}) 3055, 2962–2850, 1425, 1600, 1560, 1185, 750. Anal.% C (55.47), H (4.35), S (9.86), Cl (10.90).

2.2. Synthesis of ammine derivative of precursor compounds

*2.2.1. Synthesis of ammine derivative of precursor compound **1** (PC_1-NH_2)*

Ammonia solution (15 ml, 25%) was added into the solution of PC_1-Cl (*O*,*O*′-monoarylphosphorochloridothionate, 2.0 g) in 250 ml benzene and the temperature of the reaction was maintained below 40 °C for 2 h. The reaction mixture was cooled to room temperature and the combined extract was washed with water repeatedly to remove ammonium chloride and excess of ammonia. The organic layer was separated, dried and evaporated to give ammine derivative of precursor compound **1** (PC_1-NH_2), which was used directly for the next step (Scheme 2).

PC_1-NH_2: white powder, empirical formula $C_6H_6NO_2PS$, yield 68%, m.p. 160–162 °C. ^{1}H NMR (300 MHz, DMSO, δ) 7.06 (m, 4H, ArH), 3.40 (d, 2H, NH). FT-IR (KBr pellets ν_{max} cm^{-1}) 3324–3235, 3060, 2960–2855, 1420, 1335, 1265, 750. Anal.% C (38.53), H (3.22), N (7.47), S (17.12).

*2.2.2. Synthesis of ammine derivative of precursor compound **2** (PC_2-NH_2)*

Following the above procedure an ammonia solution was added into the solution of PC_2-Cl in a three-necked flask

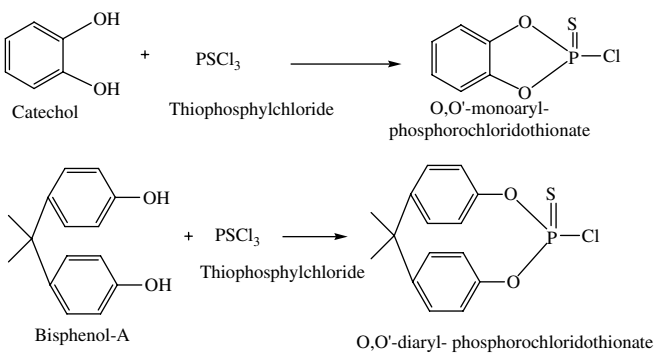

Scheme 1. Synthesis of chloride derivatives, PC_1-Cl and PC_2-Cl.

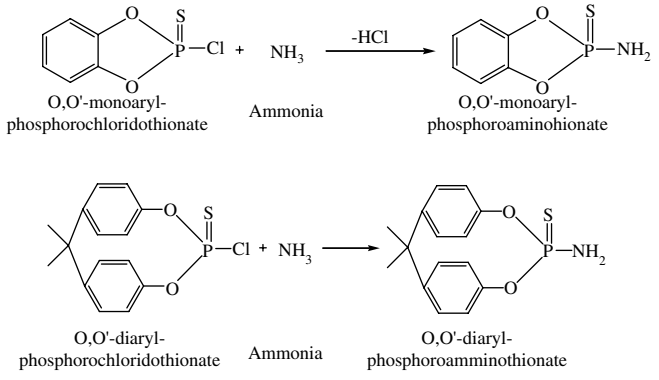

Scheme 2. Synthesis of ammine derivatives, PC_1-NH_2 and PC_2-NH_2.

equipped with stirrer, stopper funnel, and condenser. Dry benzene (250 ml) was added into this solution, while maintaining the reaction temperature below 40 °C for 2 h. The byproduct, ammonium salt was thoroughly washed with distilled water, dried over anhydrous Na_2SO_4, and the solvent evaporated in vacuum. The crude product PC_2-NH_2 was purified and recrystallized with ethanol (Scheme 2).

PC_2-NH_2: white powder, empirical formula $C_{15}H_{16}NO_2PS$, yield 61%, m.p. 163–165 °C. ^{1}H NMR (300 MHz, DMSO, δ) 6.94–7.15 (m, 8H, ArH), 1.85 (m, 6H, CH_3), 3.80 (d, NH_2). FT-IR (KBr pellets ν_{max} cm^{-1}) 3325–3230, 3050, 2962–2850, 1550, 1335, 1265. Anal.% C (59.00), H (5.29), N (4.57), S (10.51).

2.3. Synthesis of ligands, O,O′,O″,O‴-di/tetra aryldithioimidophonates (H_1L_1/H_1L_2)

NaH (sodium hydride) (5 g) in paraffin (80%) was slowly added to a well-stirred solution of 0.1 mol of ammine derivative of precursor compounds (PC_1-NH_2/PC_2-NH_2) and 100 ml anhydrous THF. Following refluxing for 2 h, the monosodium salt of PC_1-NH_2/PC_2-NH_2 was formed. Then a solution of chloride derivatives of precursor compounds (PC_1-Cl/PC_2-Cl), 0.1 mol in 100 ml anhydrous THF was added dropwise to the above suspension and the mixture was refluxed for another 6 h. Then the solvent was evaporated, the residue was diluted with 200 ml benzene, and washed with dilute hydrochloric acid (5%) and then water. The mixture was dried over Na_2SO_4. The respective colored compounds were recrystallized from ethanol and benzene (Scheme 3).

H_1L_1: light yellow, empirical formula $C_{12}H_9O_4NP_2S_2$, yield 70%, m.p. 98–101 °C. Anal.% C (40.36), H (2.53), N (3.88), S (17.98).

H_1L_2: yellow brown, empirical formula $C_{30}H_{29}O_4NP_2S_2$, yield 68%, m.p. 110–112 °C. Anal.% C (60.52), H (4.91), N (2.34), S (10.76).

2.4. Synthesis of transition metal complexes [$(H_1L_1)_2$/$(H_1L_2)_2$M(II)]

The metal complexes of H_1L_1/H_2L_2 ligands with transition metal ions were prepared according to the earlier reported method [20]. 0.02 mol of H_1L_1 (71.4 g)/H_2L_2 (23.80 g) was dissolved in 50 ml THF. To this solution tetrahydrofuran solution of $Ni(CH_3COO)_2 \cdot 4H_2O$, 2.48 g (0.01 mol) was added with continuous stirring. The color of the solution changed and the pH was adjusted to 5–5.5. The turbid mixture was stirred at 60 °C for 2 h, in order to obtain the fused product of the metal complexes. The obtained precipitate was filtered, washed with distilled water, ethanol and diethyl ether respectively, and dried in vacuum oven. The metal complexes of Mn(II), Co(II), Cu(II), and Zn(II) were synthesized by mixing 2.45, 2.49, 1.99 and 2.19 g of metal ions, respectively, with ligands in 2:1 (ligand:metal) molar ratio by similar method as mentioned above. The respective colored compounds were filtered, washed and dried (Scheme 4).

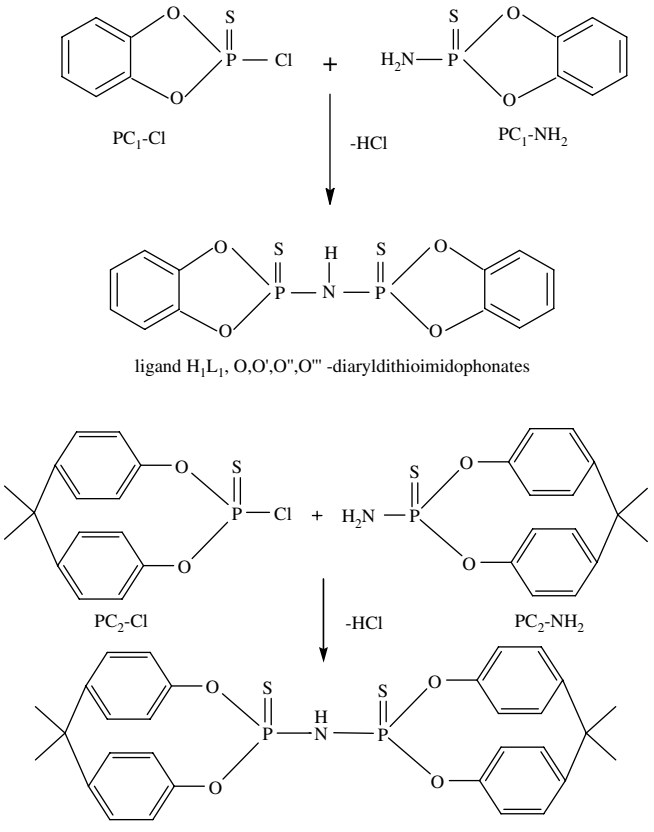

Scheme 3. Synthesis of ligand H_1L_1 and ligand H_1L_2.

$(L_1)_2$-Mn: light pink, empirical formula $C_{24}H_{14}O_8N_2P_4S_4Mn$, yield 75%, m.p. 135d. Anal.% C (37.58), H (1.85), N (3.65), S (16.72), M (7.16).

$(L_2)_2$-Mn: light pink, empirical formula $C_{60}H_{56}O_8N_2P_4S_4Mn$, yield 76%, m.p. 167d. Anal.% C (57.85), H (4.45), N (2.09), S (10.24), M (4.18).

$(L_1)_2$-Co: green, empirical formula $C_{24}H_{14}O_8N_2P_4S_4Co$, yield 80%, m.p. 138d, Anal.% C (37.34), H (2.07), N (3.65), S (16.60), M (7.64).

$(L_2)_2$-Co: dark green, empirical formula $C_{60}H_{56}O_8N_2P_4S_4Co$, yield 78%, m.p. 138d, Anal.% C (57.75), H (4.46), N (2.25), S (10.26), M (4.76).

$(L_1)_2$-Ni: olive green, empirical formula $C_{24}H_{14}O_8N_2P_4S_4Ni$, yield 79%, m.p. 137d. Anal.% C (37.35), H (2.07), N (3.65), S (16.60), M (7.66).

$(L_2)_2$-Ni: olive green, empirical formula $C_{60}H_{56}O_8N_2P_4S_4Ni$, yield 75%, m.p. 165d. Anal.% C (57.75), H (4.48), N (2.24), S (10.24), M (4.68).

$(L_1)_2$-Cu: dark brown, empirical formula $C_{24}H_{14}O_8N_2P_4S_4Cu$, yield 76%, m.p. 165d. Anal.% C (37.95), H (2.13), N (3.65), S (16.90), M (8.38).

$(L_2)_2$-Cu: dark brown, empirical formula $C_{60}H_{56}O_8N_2P_4S_4Cu$, yield 75%, m.p. 168d. Anal.% C (57.56), H (4.52), N (2.24), S (12.19), M (5.08).

$(L_1)_2$-Zn: white, empirical formula $C_{24}H_{14}O_8N_2P_4S_4Zn$, yield 78%, m.p. 135d. Anal.% C (37.83), H (2.14), N (3.67), S (16.82), M (8.57).

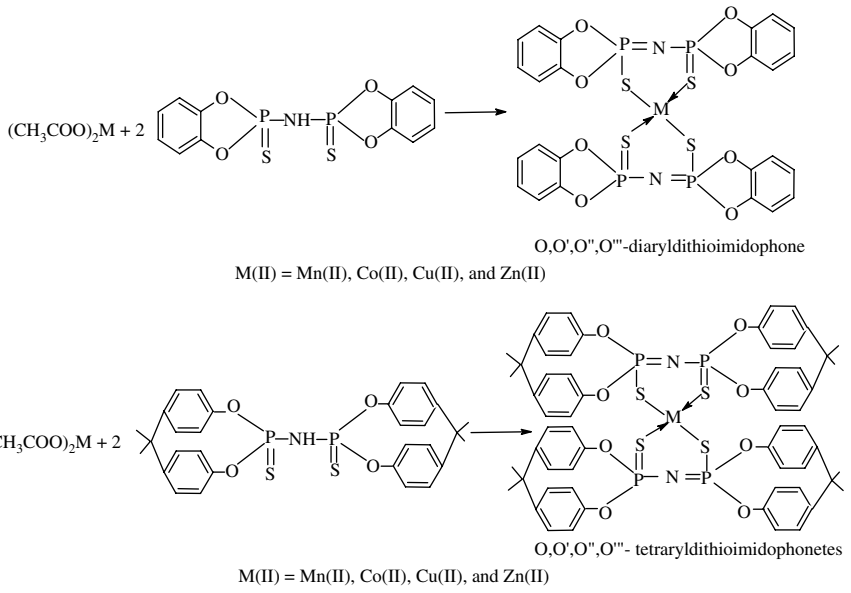

Scheme 4. Synthesis of metal complexes $[(H_1L_1/H_1L_2)_2M(II)]$.

$(L_2)_2$-Zn: white, empirical formula $C_{60}H_{56}O_8N_2P_4S_4Zn$, yield 78%, m.p. 167d. Anal.% C (57.46), H (4.54), N (2.27), S (10.30), M (5.08).

d = decomp. temp. (°C).

3. Experimental protocols

3.1. General remarks

All chemicals and solvents used were of reagent grade. Solvents were dried and distilled before use according to the standard procedure. Redistilled and deionised water was used wherever it was needed.

Melting points were determined by open capillaries in electrical melting point apparatus and are uncorrected.

Microanalysis of carbon, nitrogen and hydrogen was carried out on a Perkin Elmer model-2400 elemental analyzer.

FT-IR spectra were recorded on a Perkin–Elmer FT-IR 621 spectrometer (4000–400 cm^{-1}) using potassium bromide pellets. Electronic spectra were recorded at room temperature on a Perkin–Elmer Lambda EZ-201 UV/vis spectrophotometer as solution in DMSO. ^1H and ^{13}C NMR spectra of the ligand and its complex were recorded in DMSO-d_6 on a Bruker Spectrospin DPX-300 MHz NMR instrument at room temperature using TMS as internal standard. Molar conductivity of 10^{-3} M solution of the solid complexes in DMSO was measured on a corning conductivity meter NY 14831 model 441. Magnetic moments were measured on vibrating sample magnetometer (model 155) at USIC, Indian Institute of Technology, Roorkee. ^{31}P NMR spectra of the compounds synthesized in the present study were recorded on a 270 MHz spectrometer using DMSO as solvent and H_3PO_4 as an external standard.

In the present study, we have synthesized *O,O′*-monoarylphosphorochloridothionate (PC_1-Cl) and *O,O′*-diarylphosphorochloridothionate (PC_2-Cl) by the direct treatment of thiophosphyl chloride ($PSCl_3$) with catechol and bisphenol-A, respectively, but surprisingly, $PSCl_3$ does not react with phenolic group even under forcing conditions. In the presence of aluminum chloride, catechol and $PSCl_3$ remain unchanged after 2 h at reflux. But in the presence of NaOH or triethylamine, as an acid acceptor $PSCl_3$ reacts with equivalent catechol and *O,O′*-monoarylphosphorochloridothionate (PC_1-Cl) is prepared in moderate yield. Furthermore, the formation of byproducts such as diaryl derivatives $[(ArO)_2P(S)Cl_2]$ and thiophosphates $[(ArO)_3P(S)]$ is difficult to avoid. In an attempt to improve the yields of the reactions, phase transfer catalysts (PTC) such as tetra butyl ammonium bromide (TBAB) and benzyl triethyl ammonium chloride (BTAC) have been used [21,22]. As expected, the yields of PC_1-Cl and PC_2-Cl were enhanced up to about 80%. The chloride derivatives of PC_1 and PC_2 are crystalline solids soluble in common organic solvents. The ammine derivatives of PC_1 and PC_2 were synthesized by the reaction of ammonia with PC_1-Cl and PC_2-Cl solutions. Ligands H_1L_1 and H_1L_2 (*O,O′,O″,O‴*-diaryldithioimidophonates/*O,O′,O″,O‴*-tetra aryldithioimidophonates) were synthesized by the reaction of ammine derivatives of precursor compounds with chloro derivatives in the presence of sodium hydride (NaH). All the metal complexes are colored crystalline solids, the complexes of Mn(II), Co(II), Ni(II), Cu(II) and Zn(II) are light pink, green, olive green, dark brown and white, respectively, and insoluble in common organic solvents. Formation of precursor compounds and, subsequently, metal complexes can be summarized as follows:

$$PC_1\text{-}Cl + NH_3 \rightarrow PC_1\text{-}NH_2 \qquad PC_2\text{-}Cl + NH_3 \rightarrow PC_2\text{-}NH_2$$
$$PC_1\text{-}Cl + PC_1\text{-}NH_2 \rightarrow H_1L_1 \qquad PC_2\text{-}Cl + PC_2\text{-}NH_2 \rightarrow H_1L_2$$
$$H_1L_1 + M(CH_3COO)_2 \rightarrow (L_1)_2M + CH_3COOH$$
$$H_1L_2 + M(CH_3COO)_2 \rightarrow (L_2)_2M + CH_3COOH$$

4. Results and discussion

4.1. FT-IR study

Characteristic IR absorption frequencies with their assignments of the ligands (H_1L_1 and H_1L_2) and their metal complexes are given in Table 1. Medium weak bands in the region 3150–3350 cm^{-1} and other medium bands at 1370 cm^{-1} were assigned to NH stretching in both ligands, which are not present in the deprotonated complexes [23]. Therefore, the ligands are protonated in the same way at nitrogen, although sulfur, being more electronegative than nitrogen, might preferably bind to H. π-Bonding capabilities of P═S *vs* P═N may favor the former bond. In both the ligands two bands are common in the regions 3045–3058 and 925–980 cm^{-1} and have been ascribed to the in-plane deformation vibrations, due to aromatic C═C and P–N–P, respectively [24]. The frequency of P–N–P band increases by about 300 cm^{-1}, when the NH proton is removed. The PN bond order can be understood from the figure given below. A broad and very strong IR band at 1170–1230 cm^{-1} region in metal complexes is assigned to P……N……P.

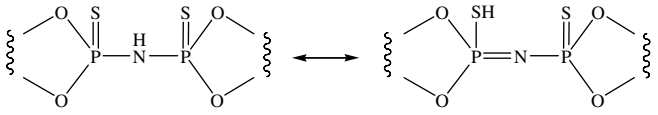

In H_1L_2 ligand the presence of methyl group was confirmed by the appearance of two strong bands at 2945–2940 and 2870–2860 cm^{-1} due to νCH symmetric and asymmetric stretching vibrations [25] and a band at 1410 cm^{-1} due to δCH_2 bending mode. The same band was not found in the spectrum of ligand H_1L_1. A very strong band in the region 795–1067 cm^{-1} has been attributed to P═S. Two new bands at 650–680 and 515–525 cm^{-1} in the spectrum of complexes are possible assignment for P……S. All the metal complexes exhibited around 70 cm^{-1} decrease in P–S frequencies upon metal chelation. In the far-IR spectra of the complexes, additional bands in the 320–410 cm^{-1} region, as compared to the ligands, are ascribable to the M–S stretching mode [26].

4.2. ^{1}H NMR spectral study

The ^{1}H NMR spectra of H_2L_1 and H_2L_2 and their Zn(II) metal complexes are recorded. The ^{1}H NMR spectrum of these ligands showed signals at 5.76 and 5.74 ppm for H_1L_1 and H_1L_2, respectively, and are assigned for NH protons [27].

The resonance signals of aromatic region are observed as multiplets in the range of 6.55–7.16 ppm in both the ligands. In the case of metal complexes a visual evaluation of signals of equal number of aromatic protons was observed due to the intermolecular interaction towards metal ions and variation in the π electron density around the protons.

The ^{1}H NMR spectrum of H_2L_2 showed an additional strong signal at 1.86 ppm attributed to the methyl protons of bisphenol-A (CH_3–C–CH_3) [28]. The absence of the NH signal in the $(L_1)_2$–Zn(II)/$(L_2)_2$–Zn(II) spectra shows the ligands in their deprotonated form and suggests possible coordination of metal ions to sulfur.

4.3. ^{13}C NMR and ^{31}P NMR spectral study

The ^{13}C NMR spectra of the ligands and their Zn(II) metal complexes display several different signals assigned to the carbons. The peaks at 146.6–115 ppm and 150–118 ppm are due to the aromatic carbons of catechol-based ligand (H_1L_1) and bisphenol-A-based ligand (H_1L_2), respectively [29].

In the spectra of Zn(II) complexes these signals showed downfield shift from their original position indicating coordination with the central metal atom. In case of H_2L_2 and L_2–Zn(II) a sharp peak observed at 18.4 ppm is assigned to the CH_3 function, which was not observed in the spectra of H_1L_1 and $(L_1)_2$–Zn(II). It was observed that DMSO did not have any coordinating effect on the spectra of metal complexes.

The ^{31}P NMR study also supports the proposed structure of the compounds. As reported earlier the position of the ^{31}P chemical shifts is not influenced by the paramagnetic nature of the metal ions. The ^{31}P spectra of H_1L_1 and H_1L_2 showed signals at 50.6 and 50.7 ppm, respectively. In the case of

Table 1
IR spectral band assignments of the ligands and their metal complexes

Compounds	Assignments (cm^{-1})						
	ν(N–H)	ν(Ar-CH)	–CH (sym.) (asym.)	ν(C═C)	ν(P═N)	ν(P═S)	ν(M–S)
H_1L_1	3155–3348(b)	3058(m)	–	1575(s)	1168(m)	795(s)	–
H_1L_2	3150–3350(b)	3052(m)	2945–2860(m)	1530(s)	1240(m)	1067(s)	–
$(L_1)_2$–Mn	3156–3345(b)	3045(m)	–	1574(s)	1160(m)	525(s)	360(s)
$(L_2)_2$–Mn	3150–3350(b)	3055(m)	2945–2865(m)	1530(s)	1240(m)	655(s)	340(s)
$(L_1)_2$–Co	3155–3340(b)	3052(m)	–	1575(s)	1162(m)	518(s)	335(s)
$(L_2)_2$–Co	3152–3350(b)	3050(m)	2942–2865(m)	1550(s)	1240(m)	675(s)	320(s)
$(L_1)_2$–Ni	3150–3345(b)	3052(m)	–	1570(s)	1160(m)	515(s)	400(s)
$(L_2)_2$–Ni	3150–3350(b)	3050(m)	2945–2870(m)	1530(s)	1240(m)	680(s)	385(s)
$(L_1)_2$–Cu	3152–3350(b)	3055(m)	–	1575(s)	1162(m)	520(s)	410(s)
$(L_2)_2$–Cu	3150–3345(b)	3050(m)	2940–2863(m)	1540(s)	1245(m)	650(s)	375(s)
$(L_1)_2$–Zn	3155–3348(b)	3052(m)	–	1575(s)	1160(m)	520(s)	370(s)
$(L_2)_2$–Zn	3150–3350(b)	3045(m)	2945–2860(m)	1535(s)	1243(m)	665(s)	375(s)

s, strong; m, medium; w, weak; sym, symmetric; asym, asymmetric.

complexes the ^{31}P spectra of $(L_1)_2$–Zn(II) and $(L_2)_2$–Zn(II) showed signals at 46.4 and 48.2 ppm, respectively [30]. These signals are actually shifted downfield due to the drifting of environmental electrons towards the metal ions.

4.4. Magnetic susceptibility studies

For the complex $(L_1)_2$–Mn(II) the measured room temperature magnetic moment value (Table 2) has been found to be 5.19 B.M. The measured magnetic moment value for $(L_2)_2$–Mn(II) has been found to be 5.23 B.M. which is intermediate between those for high-spin and low-spin species due to an $S = 5/2$ ($^6A_1$) $\leftrightarrow$ $S = 1/2$ ($^2T_2$). The observed magnetic moment values of 5.19 and 5.23 B.M. in the complexes $(L_1)_2$–Mn(II) and $(L_2)_2$–Mn(II) show five unpaired electrons and may thus be attributed to a tetrahedral geometry around Mn(II) [31], which results in a doublet ($^2T_{2g}$) $\leftrightarrow$ sextet ($^6A_{1g}$) spin-crossover phenomenon. The complexes of Co(II) in the present investigation exhibit room temperature magnetic moment values of 2.1 and 2.2 B.M. for $(L_1)_2$–Co(II) and $(L_2)_2$–Co(II), respectively. These values lie in the range of values corresponding to square planar stereochemistry around cobalt(II) d^7 complexes [32]. The square planar complexes of bivalent cobalt so far investigated are all of the low-spin type with room temperature magnetic moment values in the range 2.1–2.8 B.M. corresponding to one unpaired electron in the highest filled molecular orbital ^4A_g. Spin–orbit coupling gives some orbital contribution to the moment by mixing the higher ligand field states in the ^2A_g ground state. Room temperature magnetic susceptibility measurements give $\mu_{eff} = 0.4$ and 0.6 B.M. for $(L_1)_2$–Ni(II) and $(L_2)_2$–Ni(II). Generally, nickel(II), a d^8 system, prefers a low-spin planar geometry with diamagnetic behavior, while for a tetrahedral system, the theoretical magnetic moment (3.9 B.M.) is too high to correspond to the present nickel(II) complex. The paramagnetism in the above-said complex can be attributed to the existence of a mixture of singlet ($S = 0$) and triplet ($S = 1$) states where the singlet is the ground state and the triplet is the low-lying excited state. Such type of anomalous magnetic behavior has been observed earlier for square planar nickel(II) complexes [16]. Though d^8 square planar complexes are expected to be, in general, diamagnetic, the presence of a mixture or an equilibrium between spin-free (triplet state, two unpaired electrons would be present) and spin-paired (singlet state, no unpaired

Table 2
Electronic spectra, magnetic moments and ligand field parameters of the complexes

Compounds	Magnetic moment (B.M.)	Electronic transition (cm^{-1})	Assignment	Geometry
$(L_1)_2$–Mn	5.19	29,050	Charge transfer	Tetrahedral
		19,895	$^2A_{1g}$, $^2T_{1g} \leftarrow {}^2T_{2g}$	
		15,235	$^4T_{2g} \leftarrow {}^6A_{1g}$, $^4T_{2g} \leftarrow {}^2T_{2g}$	
$(L_2)_2$–Mn	5.23	29,070	Charge transfer	Tetrahedral
		20,050	$^2A_{1g}$, $^2T_{1g} \leftarrow {}^2T_{2g}$	
		15,380	$^4T_{2g} \leftarrow {}^6A_{1g}$, $^4T_{2g} \leftarrow {}^2T_{2g}$	
$(L_1)_2$–Co	2.10	29,130	Charge transfer	Square planar
		24,620	$^2B_{3u} \leftarrow {}^2A_g$	
		20,560	$^2B_{2u} \leftarrow {}^2A_g$	
		15,720	$^2B_{1g} \leftarrow {}^2A_{1g}$ ($xy \leftarrow x^2 - y^2$) and $^2B_{1g} \leftarrow {}^2A_g$	
$(L_2)_2$–Co	2.20	29,230	Charge transfer	Square planar
		24,740	$^2B_{3u} \leftarrow {}^2A_g$	
		20,160	$^2B_{2u} \leftarrow {}^2A_g$	
		15,210	$^2B_{1g} \leftarrow {}^2A_{1g}$ ($xy \leftarrow x^2 - y^2$) and $^2B_{1g} \leftarrow {}^2A_g$	
$(L_1)_2$–Ni	0.42	25,720	$^1B_{3u} \leftarrow {}^1A_g$	Square planar
		22,471	$^1B_{2u} \leftarrow {}^1A_g$	
		20,005	$^1B_{3g} \leftarrow {}^1A_g$	
		15,600	$^1B_{1g} \leftarrow {}^1A_g$	
$(L_2)_2$–Ni	0.61	25,740	$^1B_{3u} \leftarrow {}^1A_g$	Square planar
		22,475	$^1B_{2u} \leftarrow {}^1A_g$	
		20,020	$^1B_{3g} \leftarrow {}^1A_g$	
		15,720	$^1B_{2u} \leftarrow {}^1A_g$	
$(L_1)_2$–Cu	1.58	23,340	Charge transfer due to $^2A_{2u}$ and $^2A_g \leftarrow {}^2B_{1g}$	Square planar
		19,050	$^2B_{3g} \leftarrow {}^2B_{1g}$	
		15,265	$^2A_{1g} \leftarrow {}^2B_{1g}$	
$(L_2)_2$–Cu	1.56	23,220	Charge transfer due to $^2A_{2u}$ and $^2A_g \leftarrow {}^2B_{1g}$	Square planar
		18,670	Charge transfer	
		14,984	$^2A_{1g} \leftarrow {}^2B_{1g}$	

electron) configurations is not forbidden, especially if the $dx^2 - y^2$ orbital is not highly destabilized where the ground state changes from singlet to triplet. Due to closeness of these two levels, there could be a thermal population in both levels, which may result in an intermediate magnetic moment for the present complex. The room temperature magnetic moment values for the copper(II) complex $(L_1)_2$–Cu(II) and $(L_1)_2$–Cu(II) are 1.58 and 1.56 B.M. and this is indicative of one unpaired electron. Copper(II) d^9 complexes, which are ionic or weakly covalent in nature, have magnetic moment values in the range 2.2–1.9 B.M., which are higher than the spin-only value and have been attributed to spin–orbit coupling. For strongly covalent complexes, room temperature magnetic moment values are found to lie between 1.82 and 1.72 B.M. However, there is antiferromagnetism due to spin–spin coupling and, hence, low room temperature magnetic moment values (1.6–1.3 B.M.) have been observed for copper(II) complexes [33]. From the above discussion it appears that the copper(II) complex under study is strongly covalent in character, but the lower magnetic moment value indicates that copper(II) ions are antiferromagnetically coupled and, hence, the complex is square planar.

4.5. Electronic absorption spectral studies

The electronic spectra of all the synthesized metal complexes were recorded in DMSO and the corresponding bands are represented in Table 2. The solution electronic absorption spectrum of $(L_1)_2$–Mn(II) exhibits three transition bands at 29,050, 19,895, and 15,235 cm^{-1} due to charge transfer spectra (M → L and L → M), $^2A_{1g}$, $^2T_{1g} \leftarrow {}^2T_{2g}$ and $^4T_{2g} \leftarrow {}^6A_{1g}$ and $^4T_{2g} \leftarrow {}^2T_{2g}$, respectively. The complex $(L_2)_2$–Mn(II) also shows three well-defined bands in the UV/vis regions. A band at 29,070 cm^{-1} is an intense band and arises due to charge transfer transitions. The other two bands at 20,050 and 15,380 cm^{-1} are of medium intensity. The absorption at 20,050 cm^{-1} can be attributed to the transitions $^2A_{1g}$, $^2T_{1g} \leftarrow {}^2T_{2g}$. The broad band at 15,380 cm^{-1} may arise due to the transitions $^4T_{2g} \leftarrow {}^6A_{1g}$ and $^4T_{2g} \leftarrow {}^2T_{2g}$. The assignment of a band at 15,380/15,235 cm^{-1} to two 'd–d' transitions, its width, and symmetry have been attributed to two overlapping bands, of which the higher frequency one is characteristic of the low-spin form and the other of the high-spin form. The appearance of separate absorption band $^2T_{1g} \leftarrow {}^2T_{2g}$ at 20,050/19,895 and $^4T_{2g} \leftarrow {}^2T_{2g}$ at 15,380/15,235 cm^{-1} for the two spin-states in the electronic absorption spectrum of the complex further supports the existence of a spin-free–spin-paired ($^2T_{2g} \leftarrow {}^6A_{1g}$) equilibrium established earlier on the basis of magnetic data [31] (Table 2). The electronic spectra of $(L_1)_2$–Co(II) show four transition bands at 29,130, 24,620, 20,560 and 15,720 cm^{-1}. The presence of four electronic absorption bands instead of two generally observed for tetrahedral cobalt(II) complexes suggests a square planar geometry. In the electronic absorption spectrum of $(L_2)_2$–Co(II) in DMSO solution, four bands at 29,230, 24,740, 20,160 and 15,210 cm^{-1} were observed and show square planar geometry. A well-defined strong band occurring at 15,720/15,210 cm^{-1} is assigned to the transition $^2B_{1g} \leftarrow {}^2A_g$ ($x^2 - y^2 \rightarrow xy$) and $^2B_{3g} \leftarrow {}^2A_g$. A shoulder around 20,560/20,160 cm^{-1} and another strong band at 24,620/24,740 cm^{-1} are assigned to the $^2B_{2u} \leftarrow {}^2A_g$ and $^2B_{3u} \leftarrow {}^2A_g$ metal-to-ligand charge transfer transitions, respectively. The solution electronic absorption spectrum of the nickel(II) d^8 complex consists of four absorption bands for both the ligands. Electronic spectra of square planar nickel(II) with H_1L_1 show transitions at 25,720, 22,471, 20,005, and 15,600 cm^{-1}, the lowest energy band lying at 15,600 cm^{-1} is assigned to the parity-forbidden $^1B_{1g} \leftarrow {}^1A_g$ transition, and the higher energy band at 20,005 cm^{-1} to the $^1B_{3g} \leftarrow {}^1A_g$ transition. The shoulder at 22,471 cm^{-1} and a strong band at 25,720 cm^{-1} are assigned to metal-to-ligand charge transfer $^1B_{2u} \leftarrow {}^1A_g$ and $^1B_{3u} \leftarrow {}^1A_g$ transitions, respectively [34], while in the electronic spectra of $(L_2)_2$–Ni(II) complexes these bands occur at 25,740, 22,475, 20,020 and 15,720 cm^{-1}. In the solution electronic absorption spectrum of the complex $(L_1)_2$–Cu(II), three absorption bands were observed at 23,340, 19,050 and 15,265 cm^{-1}. The lowest energy band at 15,265 cm^{-1} is a band of medium intensity and is considered to be the only d–d band. It is assigned to $^2A_{1g} \leftarrow {}^2B_{1g}$ transition. The band at 23,340 cm^{-1} is a composite one (d–d and CT) due to the ^2A_u and $^2A_g \leftarrow {}^2B_{1g}$ transitions. This band is very strong, broad and unsymmetrical and seems to contain another allowed charge transfer band on the higher energy side at 29,240 cm^{-1}, due to the $^2B_{1u} \leftarrow {}^2A_{1g}$ transition. On the lower energy side of this band, a very weak shoulder at 19,050 cm^{-1} may be attributed to the $^2B_{3g} \leftarrow {}^2B_{1g}$ d–d transition. The electronic spectra of the $(L_2)_2$–Cu(II) complex exhibit three bands at 14,984, 18,670 and 23,220 cm^{-1}, due to $^2A_{1g} \leftarrow {}^2B_{1g}$(F), $^2B_{3g} \leftarrow {}^2B_{1g}$ and charge transfer which indicate square planar geometry [34].

5. Pharmacology

5.1. Antimicrobial susceptibility testing

Antibacterial activity of the prepared compounds was investigated against the standard strains: *Escherichia coli*, *Bacillus subtilis*, *Staphylococcus aureus* and the antifungal activity against the standard strains: *Aspergillus flavus*, *Aspergillus niger*, and *Candida albicans*. Minimum inhibitory concentrations (MICs) of antimicrobial agents for the isolates were determined *in vitro* as described by Clause [35]. Kanamycin was used for antibacterial activity and Miconazole was used for antifungal activity as standards. The stock solutions (3.00 mg/ml) of the test compounds and reference drugs were initially prepared by dissolving 30 mg in 10 ml DMSO and serially diluted to 1.50, 0.75, 0.37, 0.18, 0.09, 0.04, 0.02, 0.01 and 0.005 mg/ml using nutrient broth. Nutrient broth (pH 6.9) and Muller Hinton agar medium (pH 7.2) were provided by their manufacturer (Hi Media Lab. Pvt. Ltd) for use in this study. The antimicrobial agents with their various concentrations inoculated with each isolate were incubated at 35 °C in ambient air for 24–48 h. After the incubation the growth of the pathogen was determined visually for both antimicrobial agents and controls. The lowest concentration

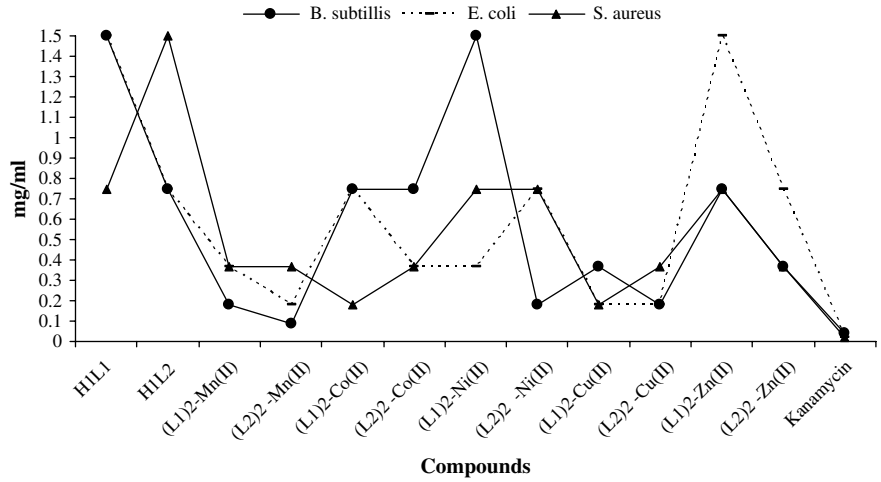

Fig. 1. MICs of the ligands and their metal complexes against bacteria (MIC values were determined as mg/ml active compounds in medium).

at which there was no visible growth (turbidity) for each chemical compound was recorded as minimum inhibitory concentration (MIC).

5.2. Biological results

The minimum inhibitory concentrations of the compounds against bacteria and fungi are shown in Figs. 1 and 2.

As shown in Fig. 1, the ligands exhibited weak antibacterial activity with respect to the complexes. Ligands exhibited MICs in the range of 0.75–1.5 mg/ml. Complex $(L_2)_2$–Mn(II) showed effective antibacterial activity against *B. subtilis* (MIC, 0.09 mg/ml). Complexes of Mn(II) and Cu(II) showed moderate inhibitory activity against the pathogens (MIC 0.18–0.37 mg/ml), however, the results indicate slight differences between the activities of all the complexes.

According to the antifungal minimum inhibitory concentration results (Fig. 2), ligand H_1L_1 showed reliable inhibitory activity against *C. albicans*. $(L_1)_2$–Cu(II) complex exhibited the most potent and well-balanced activity against the pathogens.

All compounds exhibited moderate to good activity against both bacteria and fungi. Although all the compounds are active, they did not reach the effectiveness of conventional standards Kanamycin and Miconazole. The variation in effectiveness of different compounds against different organisms depends either on impermeability of cells of the microbes or diffusion in the ribosome of microbial cells [36]. This investigation revealed that the ligands are more active when they were treated against fungi. All the complexes exhibited improved antimicrobial activity than their parent ligands. Several studies reported that the metal complexes of divalent cations are more toxic than their metallic forms, particularly when compared to their own inorganic equivalents [37]. It may be due to chelation of metal because chelation reduces the polarity of the central metal ion by partial sharing of its positive charge with the donor groups. This process increases the lipophilic nature of the central metal ion, which in turn favors its permeation into the lipid layer of the membrane.

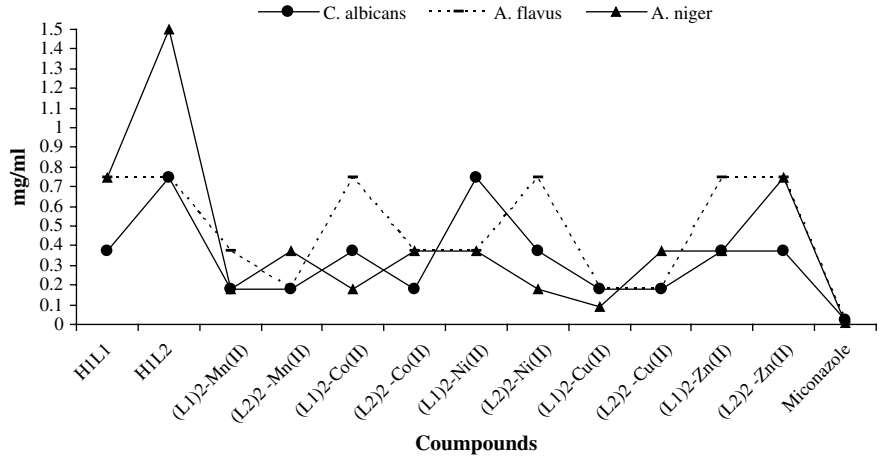

Fig. 2. MICs of the ligands and their metal complexes against fungi (MIC values were determined as mg/ml active compounds in medium).

References

[1] L.F. Jin, F.P. Xiao, G.Z. Cheng, Z.P. Ji, J. Organomet. Chem. 691 (2006) 2909–2914.
[2] G.A. Bogdanovic, A.S. Bire, B.V. Prelesnik, V.M. Leovac, Acta Crystallogr., C 54 (1998) 766–768.
[3] D. Maganas, S.S. Staniland, A. Grigoropoulos, F. White, S. Parsons, N. Robertson, P. Kyritsis, G. Pneumatikakisa, Dalton Trans. (2006) 2301–2315.
[4] I.H. Hall, C.B. Lackey, T.D. Kistler, R.W. Durham, J.M. Russell, R.N. Grimes, Anticancer Res. 20 (2000) 2345–2354.
[5] M.E. Vol'pin, G.N. Novodarova, N.Yu. Krainova, V.P. Lapikova, A.A. Aver'yanov, J. Inorg. Biochem. 81 (2000) 285–292.
[6] A. Bravo, J.R. Anacona, Trans. Met. Chem. 26 (2001) 20–23.
[7] D. Kovala-Demertzi, J. Inorg. Biochem. 79 (2000) 153–157.
[8] P. Bindu, M.R.P. Kurup, T.R. Satyakeerty, Polyhedron 18 (1999) 321–331.
[9] J.A. Darr, M.P. Poliakoff, W.S. Li, A.J. Blake, J. Chem. Soc., Dalton Trans. (1997) 2869–2874.
[10] J.A. Darr, M.P. Poliakoff, A.J. Blake, W.S. Li, Inorg. Chem. 37 (1998) 5491–5496.
[11] A. Schmidpeter, H. Groeger, Z. Anorg. Allg. Chem. 345 (1966) 106–110.
[12] A. Schmidpeter, J. Ebeling, Chem. Ber. 101 (1968) 815–823.
[13] I. Haiduc, J. Organomet. Chem. 623 (2001) 29–42.
[14] R. Rösler, C. Silverstru, G. Espinosa-Pérez, I. Haiduc, R. Cea-Olivares, Inorg. Chim. Acta 241 (1996) 47–54.
[15] J.O. Morley, M.H. Charlton, J. Phys. Chem. A 102 (1998) 6871–6876.
[16] E. Simón-Manso, M. Valderrama, D. Boys, Inorg. Chem. 40 (2001) 3647–3649.
[17] C. Silvestru, R. Rösler, J.E. Drake, J. Yang, G. Espinosa-Pérez, I. Haiduc, J. Chem. Soc., Dalton Trans. (1998) 73–78.
[18] N. Sridevi, K.K.M. Yusuff, Toxicol. Mech. Methods 17 (2007) 559–565.
[19] D. Sellmann, H. Binder, D. Haubinger, F.W. Heinemann, J. Sutter, Inorg. Chim. Acta 300–302 (2000) 829–836.
[20] S.A. El-Shatoury, High Perform. Polym. 7 (1995) 433–438.
[21] S. Mallakpour, Z. Rafiee, Eur. Polym. J. 43 (2007) 1510–1515.
[22] P. Sharma, A. Kumar, M. Sharma, Catal. Commun. 7 (2006) 611–617.
[23] B.L. Rivas, G.V. Seguel, K.E. Geckeler, Angew. Makromol. Chem. 238 (1996) 1–10.
[24] O. Kühl, S. Blaurock, J. Sieler, E. Hey-Hawkins, Polyhedron 20 (2001) 111–117.
[25] N. Nishat, M.M. Haq, T. Ahmad, V. Kumar, J. Coord. Chem. 60 (2007) 85–96.
[26] K. Fujisawa, S. Imai, S. Suzuki, Y. Moro-oka, Y. Miyashita, Y. Yamada, K. Okamoto, J. Inorg. Biochem. 82 (2000) 229–238.
[27] R. Jayakumar, M. Rajkumar, R. Nagendran, S. Nanjundan, J. Macromol. Sci., Part A: Pure Appl. Chem. 38 (2001) 869–888.
[28] R.M. Silverstein, G.C. Basler, C.T. Morrill, Spectrometric Identification of Organic Compounds, fifth ed. Wiley Interscience, New York, 1991.
[29] P. Ghosh, R. Shukla, D.K. Chand, P.K. Bharadwaj, Tetrahedron 51 (1995) 3265–3270.
[30] W. Kemp, Proton NMR Spectra: NMR in Chemistry, first ed. McMillan Education Ltd, London, 1996.
[31] N. Bhojak, D.D. Gudasaria, N. Khiwani, R. Jain, Eur. J. Chem. 4 (2007) 232–237.
[32] B.S. Manhas, B.C. Verma, S.B. Kalia, Polyhedron 14 (1995) 3549–3556.
[33] N. Raman, V. Muthuraj, S. Ravichandran, A. Kulandaismy, Proc. Indian Acad. Sci. (Chem. Sci.) 115 (2003) 161–167.
[34] B.N. Figgis, Introduction to Ligand Fields, Interscience Publishers, Inc., New York, 1967.
[35] G.W. Clause, Understanding Microbes: A Laboratory Text Book for Microbiology, W.H. Freeman and Company, New York, 1989.
[36] P.G. Lawerence, P.L. Harold, O.G. Francis, Antibiot. Chemother. (1980) 1597–1601.
[37] K. Fent, Crit. Rev. Toxicol. 26 (1996) 1–117.